Inter-Research Science Publisher

Marine Ecology Progress Series
Volume 753:55–72

Published January 30, 2025
https://doi.org/10.3354/meps14769

Inorganic nitrogen pathways in oyster holobionts and underneath sediments studied via ^{15}N-based methods

Samuele Pagani[1,2,*], Sara Benelli[1], Marco Bartoli[1,3]

[1]Department of Chemistry, Life Sciences and Environmental Sustainability, University of Parma, Parco Area delle Scienze 33/A, 43124 Parma, Italy

[2]International Marine Centre — IMC Foundation, Loc. Sa Mardini 09170, Torregrande, Oristano, Italy

[3]Department of Integrative Marine Ecology, Stazione Zoologica Anton Dohrn, Genoa Marine Centre, Villa del Principe, Piazza del Principe 4, 16126 Genoa, Italy

ABSTRACT: Oyster biofilms have significant potential as reactors for excreted nitrogen (N) via assimilative, dissimilative and oxidative pathways. However, the interplay between molluscs, associated microbes and microalgae within biofilms is not well characterized. This work aimed to quantify dark and light oxygen (O_2) fluxes and N transformations in biofilm-colonised and biofilm-free oyster holobionts (i.e. oysters and their associated microbial communities) and to contrast N processes in oyster holobionts with those underneath the sediments. Oysters and sediments were collected from Goro Lagoon in northern Italy. Measurements were carried out in mesocosms and cores, tracing the fate of ^{15}N-labelled ammonium (NH_4^+) and nitrate (NO_3^-). We hypothesized the dominance of assimilative and dissimilative N pathways under light and dark conditions, respectively, and large stimulation of NO_3^- reduction in sediments underneath oysters due to biodeposits. Oyster holobionts, regardless of biofilm presence or absence on their outer shells and the presence or absence of illumination, were net O_2 sinks and NH_4^+ and NO_3^- sources to the water column. Biofilm photosynthesis was insufficient to contrast respiratory O_2 demand but promoted nitrification of excreted NH_4^+. Nitrification and denitrification were also recorded in biofilm-free oysters, suggesting active nitrifying and denitrifying microbial communities inside molluscs. Denitrification efficiency measured in biofilm-colonised and biofilm-free oyster holobionts was <10%, suggesting that oysters in the Goro Lagoon are weak N sinks and promote its recycling. Sediments receiving biodeposits recycled NH_4^+ at rates comparable to control sediments; however, the former displayed higher denitrification rates. N processes mediated by oyster holobionts largely exceeded those occurring in sediments.

KEY WORDS: *Magallana* (*Crassostrea*) *gigas* · Biofilm · Nitrogen recycling · Nitrification · Excretion · Denitrification

1. INTRODUCTION

The biogeochemical ecosystem services provided by oyster holobionts (i.e. oysters and the associated or symbiotic community of microorganisms growing inside the mollusc or attached to its shell) have been explored to enhance oyster reef restoration actions (Chambers et al. 2018, Ayvazian et al. 2021, Ray & Fulweiler 2021, Yu & Gan 2021). Results from laboratory and *in situ* experiments suggest that natural and restored oyster reefs, besides coupling pelagic and benthic systems, have a large potential to support the removal of reactive nitrogen (N) via denitrification (Caffrey et al. 2016, Arfken et al. 2017, Rose et al. 2021).

*Corresponding author: samuele.pagani@unipr.it

N removal via denitrification is generally addressed in sediments (i.e. in the biodeposit-enriched sediments underneath oysters) (Smyth et al. 2016). However, denitrification can be carried out by oyster holobionts, along anoxic niches inside the oysters' digestive tract (e.g. the gut) or within biofilms growing on the oyster shells, where it can be coupled to the oxidation of the excreted ammonium (NH_4^+) via nitrification (Arfken et al. 2017). Indeed, oysters form dense reef structures with densities up to 800 ind. m^{-2}, growing on the shells of dead organisms and fuelling microbial activity by producing and retaining biodeposits (Haven & Morales-Alamo 1966, Dame et al. 1992, Chambers et al. 2018, Murphy et al. 2019, Searles et al. 2022). Oyster reefs offer a large amount of surface area for biofilm colonisation (Gutiérrez et al. 2003, Ivanov et al. 2006). In shallow bays and lagoons, such biofilms may include algae, favoured by light and nutrient availability due to oyster filtration and excretion, respectively (Smaal et al. 2019). Algae may compete with microbes for N, temporarily trap the excreted NH_4^+ via uptake, and constrain net N loss via nitrification and denitrification, a biogeochemical service provided by oysters (Ray et al. 2019 and references therein). Wide availability of inorganic N can offset the competition between microalgae and microbes (Trottet et al. 2016), and the photosynthetically produced oxygen (O_2) can expand the oxic layer of the biofilm where nitrification occurs and reduce the anaerobic volume where denitrification is confined (Risgaard-Petersen et al. 2004). However, the role of biofilms growing on marine mollusc shells in N cycling is poorly documented in the literature.

In oyster reefs, the quantification of the denitrification biogeochemical service and its regulation are important in the framework of eutrophication, a naturally occurring phenomenon of coastal ecosystems, which can evolve into dystrophic conditions and mass mortality events (Viaroli et al. 2001) in the context of the negative effects of large reactive N transport to the coastal zone. To this purpose, denitrification should be studied together with other co-occurring processes involved in N cycling to address, for example, its efficiency as a net N-removing process compared to processes leading to N recycling (e.g. excretion, ammonification, nitrate ammonification or nitrification) or temporary retention (e.g. microalgal uptake). Studies targeting benthic N cycling have been carried out in sediments with burrowing molluscs such as the clams *Ruditapes philippinarum* and *Macoma baltica* (Reise 1983, Bartoli et al. 2001, Karlson et al. 2005, Michaud et al. 2006, 2009, Nizzoli et al. 2006a,b, Norkko et al. 2013, Murphy et al. 2018). They revealed that the presence of molluscs resulted in higher denitrification rates due to the microbial communities living and proliferating in specific internal organs (i.e. gut) and on the shells of molluscs. These studies also revealed a much larger stimulation of benthic NH_4^+ recycling, mostly due to direct molluscan excretion, resulting in decreased denitrification efficiency in the presence of molluscs compared to bare sediment (McMahon & Williams 1984, Bernard & Noakes 1990, Kemp et al. 1990, Nizzoli et al. 2006b, Welsh et al. 2015). Stief (2013) reviewed the net effect that burrowing macrofauna produce on benthic N cycling and concluded that NH_4^+ recycling via direct macrofaunal excretion or due to the mobilisation of pore water NH_4^+ during bioturbation often exceeds N_2 production, resulting in low denitrification efficiency. This means that only a minor fraction of the NH_4^+ produced within sediments or excreted flows through the nitrification–denitrification loop.

In this study, oyster holobionts of *Magallana* (*Crassostrea*) *gigas* (Thunberg, 1793) were collected in late winter in groups of a few individuals, hereafter referred to as aggregates, from a shallow illuminated natural reef located in the eutrophic Goro Lagoon (northern Italy), and were incubated under light and dark conditions. Dark incubation was carried out using oysters with biofilm-coated shells and repeated using oysters with the biofilm removed by gentle brushing of the shell (cleaned). Light incubation was carried out only using oysters with biofilm-coated shells to investigate the role of microalgae in O_2 and N dynamics. Cleaned oysters were not incubated in the light as biofilms were carefully removed from the shells and no differences were expected with dark incubation of cleaned oysters. Two independent sets of such light and dark incubations were carried out: one adding labelled ammonium ($^{15}NH_4^+$) and the other adding labelled nitrate ($^{15}NO_3^-$) to the water column of the incubated mesocosms.

Using dark inorganic N fluxes measured in biofilm-coated and biofilm-free aggregates, we aimed to quantify the share of O_2 respiration occurring in the biofilm and N transformations over the whole oyster holobiont respiration and N transformations, including excretion, ammonification, denitrification and nitrate ammonification. Light measurements allowed us to measure O_2 production by the biofilm, calculate the N uptake and temporary retention associated with the algal community and analyse whether microalgae inhibit or stimulate N-related microbial activity. The dilution of $^{15}NH_4^+$ allowed us to calculate NH_4^+ excretion by the molluscs, whereas the dilution of $^{15}NO_3^-$ and the production of $^{29}N_2$ and $^{30}N_2$ along the course of

the incubation allowed us to calculate the rates of nitrification and denitrification in the oyster holobionts.

Sediments that receive biodeposits (i.e. underneath and in the proximity of the oyster reef) and the oyster specimens were collected in February 2023. These, along with control sediments without biodeposits and oyster holobionts, were incubated in the darkness to contrast microbial respiration, inorganic N fluxes and rates of NO_3^- reduction.

It was hypothesized that the metabolic rate and functionality of oyster holobionts would increase in the presence of biofilm growing on oyster shells. Additionally, the impact of oyster holobionts on inorganic N fluxes is thought to depend on light availability. This is due to the assimilative activity of microalgae, which can potentially counteract the activity of both nitrifying and denitrifying microbes. Higher rates of nitrification and denitrification of excreted NH_4^+ were thus expected in the dark compared to the light biofilm-coated oysters due to lower competition between algae and microbes. It was also hypothesised that biodeposits would enhance dissimilative NO_3^- reduction in sediments underneath oyster aggregates, thereby increasing their denitrification efficiency.

2. MATERIALS AND METHODS

2.1. Oyster aggregate collection

Oyster aggregates (n = 16; 8 used in Expt 1; 8 used in Expt 2) were carefully collected by hand from a natural reef in the western corner of the Goro Lagoon (Fig. S1 in the Supplement at www.int-res.com/articles/suppl/m753p055_supp.pdf). This lagoon is shallow (average depth: 1.5 m), microtidal, eutrophic and hosts large populations of the cultivated manila clam *Ruditapes philippinarum*, mussels *Mytilus galloprovincialis* and oysters (Viaroli et al. 2006). The oyster reef area is influenced by the input of nutrient-rich freshwater from the Po di Volano, the southernmost branch of the Po River. Freshwater inputs result in an average salinity of 18 and elevated concentrations of chlorophyll *a* (chl *a*), generally exceeding 40 µg l^{-1} (Viaroli et al. 2006). During oyster sampling in February 2023, dissolved NO_3^-, NH_4^+ and reactive phosphorus concentrations were 100, 8 and 0.2 µM, respectively. Aggregates were collected and selected in order to have similar fresh weights, which averaged 306 ± 57 g aggregate^{-1}. Similar wet weight among aggregates was the only criterion identified as a proxy for the shell surface colonizable by biofilms. *In situ* aggregates had very heterogeneous shapes and included live organisms growing on old, empty shells. After pilot tests on single oyster respiration and excretion rates that were carried out to set oyster biomass and incubation times, it was decided to collect and incubate aggregates with 2–3 live oysters. However, after the incubations, all shells were opened, and aggregates sometimes included small individuals that were not accounted for. Results of measured fluxes and calculated processes were expressed on a per hour and per aggregate basis or on a per hour and per g dry weight (g_{dw}) basis of the total oyster flesh in each aggregate. At the end of the incubations, the wet flesh from each aggregate was weighed fresh and then placed in an oven at 60°C until a constant dry weight was achieved (Mo & Neilson 1994). Each aggregate included 2–6 organisms, with total dry flesh weight varying between 4 and 18 g and averaging 8.99 ± 3.95 g.

2.2. Oyster aggregates incubations: Expts 1 and 2

Oyster aggregates were incubated the day after they were collected. Incubations carried out between 24 and 48 h of sample collection are not susceptible to metabolic alterations due to starvation of the molluscs and associated biofilms that occurs after several days (Richard et al. 2006 and references therein). Aggregates were evidently colonised by biofilms (Fig. S2); upon collection, they were gently transferred to aerated 50 l tanks (4 aggregates tank^{-1}) containing *in situ* water and transported to the laboratory within 2 h, together with 600 l of *in situ* water. In the laboratory, each aggregate was transferred to cylindrical plexiglass mesocosms (n = 16; inner diameter: 20 cm; height: 40 cm, hereafter referred to as mesocosms) equipped with a water stirring system consisting of an aquarium pump (150 l h^{-1}) to avoid water stagnation. The volume of each aggregate was carefully quantified upon submersion in the mesocosm. All mesocosms were submersed with the top open in large aquaria containing fresh, aerated and stirred *in situ* water maintained at *in situ* temperature (10°C). After overnight dark pre-incubation, the water in the aquaria was fully replaced with *in situ* water to provide oysters with phytoplankton and keep nutrient concentrations close to *in situ* levels. After water replacement, incubations started according to the scheme detailed in Fig. 1a. Two sets of 4 mesocosms each were spiked with a 10 mM $^{15}NH_4^+$ solution, resulting in a final concentration of 5 µM (Expt 1). This concentration represents a 60% enrichment with labelled N of the unlabelled NH_4^+ pool, given that the *in situ* $^{14}NH_4^+$ concentration was 8.3 µM (spectropho-

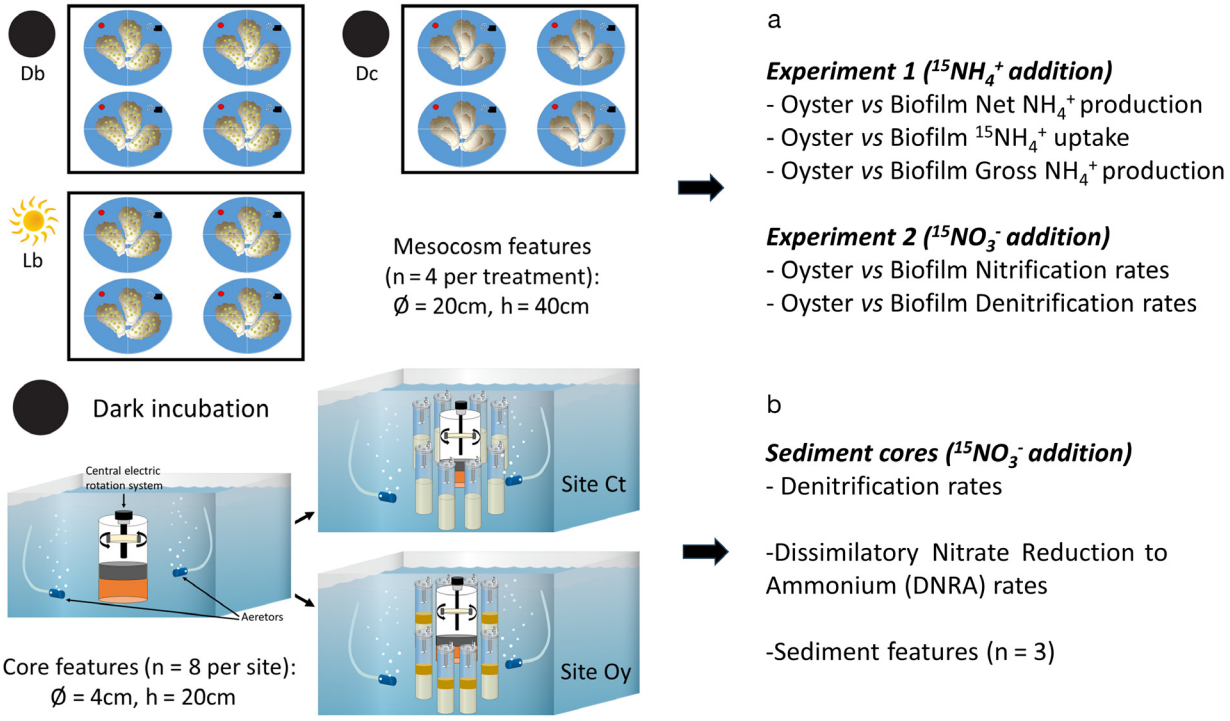

Fig. 1. (a) the Experimental mesocosms where oyster aggregates were incubated under 3 conditions: dark biofilm-coated (Db), dark cleaned (Dc) and light biofilm-coated (Lb). (b) Dark incubation of intact sediment cores underneath and in proximity of the oyster reef

tometry; Bower & Holm-Hansen 1980). One set of mesocosms (dark biofilm-coated, Db, n = 4) was incubated in the dark, while the other set (light biofilm-coated, Lb, n = 4) was incubated under light conditions using halogen lamps at an irradiance of 150 µE m^{-2} s^{-1}, which is similar to the average *in situ* light conditions in late February. A few minutes after $^{15}NH_4^+$ addition, dissolved O_2 concentration in each mesocosm was measured with a microelectrode (OX-50, Unisense) and a water subsample was collected with a 50 ml plastic syringe and filtered (Whatman, 0.7 µm glass fibre filter). An aliquot of the filtered water (10 ml) was transferred to plastic vials for spectrophotometric analysis of total dissolved NH_4^+ ($^{14}NH_4^+$ + $^{15}NH_4^+$) and another aliquot (20 ml), purged with air for 5 min to eliminate $^{29}N_2$ and $^{30}N_2$ excess produced during the incubations, was transferred to a 12 ml glass vial (Exetainer, Labco) for the determination of labelled and unlabelled NH_4^+ (Yin et al. 2014). Labelled NH_4^+ was quantified by means of its oxidation to $^{29}N_2$ and $^{30}N_2$ with hypobromite (Warembourg 1993), and the produced labelled N_2 was measured via membrane inlet mass spectrometer (MIMS Bay instrument; Kana et al. 1994). After this time zero (t_0) sampling, each mesocosm was closed with a gas-tight transparent lid. After 3.5 h of incubation, lids were removed and a second O_2 measurement and water sampling was carried out as previously described. Afterwards, the incubations continued with open mesocosms to allow gas exchange with the atmosphere and avoid further O_2 drop. A third and fourth set of measurements were carried out after 10 and 17 h from the beginning of the experiment, respectively, for tracking ^{15}N dilution through time.

All incubations started after a visual check to ensure that oysters had open shells. The first part of the incubation ($t_0 - t_1$) was designed to measure dark and light O_2 fluxes and was carried out with the mesocosms closed. Between t_0 and t_1, oyster aggregate respiration resulted in a 20–30% decrease of the initial O_2 concentration, which is acceptable and avoids limitations to aerobic processes such as nitrification (Dalsgaard et al. 2000). The latter phases of the incubation ($t_1 - t_2$ and $t_2 - t_3$) were designed to measure $^{15}NH_4^+$ and $^{14}NH_4^+$ fluxes in both dark and light conditions. Additionally, calculations were performed to measure the dilution of $^{15}NH_4^+$ with $^{14}NH_4^+$ produced by oysters (e.g. via excretion) or the biofilm, along with determining the uptake of both $^{15}NH_4^+$ and $^{14}NH_4^+$. At the end of the incubations, the aggregates incubated in the dark were retrieved from the mesocosms and brushed with toothbrushes until the biofilm growing on the shells was completely removed (Fig. S3). They were then washed with *in situ* water, pre-incubated

into fresh *in situ* water and then transferred to mesocosms for a second dark incubation (dark-cleaned, Dc) as previously described. The second dark incubation was designed to measure O_2 respiration and $^{15}NH_4^+$ and $^{14}NH_4^+$ fluxes in clean aggregates, excluding the activity of biofilms. The biofilm removed from the Db treatments was averaged between replicates and analysed for chl *a* concentration via 90% acetone extraction (see Section 2.6 for analytical procedures) for both experiments (Expts 1 and 2).

Expt 2 was carried out using 2 other sets of 4 mesocosms each, following the same approach described for Expt 1. In brief, oyster holobiont aggregates covered by biofilm were incubated under light and dark conditions; biofilms were then removed and a second dark incubation of cleaned aggregates was carried out. Each incubation consisted of 4 sampling times (t_0, t_1, t_2 and t_3); mesocosms were closed from t_0 to t_1 and remained open for the rest of the incubation. In Expt 2, mesocosms were spiked with $^{15}NO_3^-$ to measure the denitrification rates in the oyster holobiont and the dilution of labelled NO_3^- due to nitrification and production of $^{14}NO_3^-$. At t_0 and t_1, dissolved O_2 was measured using a microelectrode and 2 water samples were collected via plastic syringes. One sample (20 ml) was filtered and frozen for later determination of $^{15}NO_3^-$ and $^{14}NO_3^-$ concentrations, and a second water sample (20 ml) was transferred, unfiltered, into a 12 ml glass vial (Exetainer, Labco) and poisoned with 100 µl of $ZnCl_2$ 7 M to stop microbial activity for the determination of $^{29}N_2$ and $^{30}N_2$ abundances. At t_2 and t_3, only one water sample was collected to analyse $^{15}NO_3^-$ and $^{14}NO_3^-$ concentrations. Total nitrate (NO_3^- + NO_2^-) was measured spectrophotometrically after cadmium reduction to NO_2^- while labelled and unlabelled NO_3^- were quantified by microbial reduction to $^{29}N_2$ and $^{30}N_2$ via MIMS (APHA 1975, Carpintero Moraes et al. 2019). Denitrification rates were determined by analysing the abundances of $^{29}N_2$ and $^{30}N_2$ via MIMS (Nielsen 1992).

2.3 Expt 1: Calculations of O_2 and labelled and unlabelled NH_4^+ fluxes

O_2 fluxes (µmol O_2 aggregate^{-1} h^{-1}) were calculated as the difference between t_1 and t_0 concentrations (in µM) multiplied by the water volume of the mesocosms (in l) and divided by the incubation time (in h). Given that the molar stoichiometry between O_2 and CO_2 can be assumed to be ~1:1 in both photosynthetic and respiratory processes (Vachon et al. 2020, Jørgensen et al. 2022), and considering that oysters generally feed on phytoplankton and that at the sampling site during late winter–early spring diatoms represent the dominant algal group in the Goro Lagoon, net O_2 fluxes measured in the different treatments were converted into net potential ammonification rates (Sundbäck et al. 2000, Zilius et al. 2012). Besides the ~1:1 molar ratio between O_2 and CO_2, a 106:16 molar ratio between carbon (C) and N was assumed for diatoms (McCarthy 1980, Takeda 1998). Net potential NH_4^+ fluxes were therefore obtained by dividing O_2 fluxes by 7. As oysters can feed also on more refractory organic particles, characterised by C:N ratios above 7, the calculated potential ammonification rates set the upper threshold for NH_4^+ production by the oyster holobiont aggregates.

The net flux of NH_4^+ (µmol NH_4^+ aggregate^{-1} h^{-1}) was calculated from the slope of the linear regression between the spectrophotometric measurement of the NH_4^+ concentration (in µM) and the incubation time (in h) multiplied by the water volume of the mesocosms (in l). The $^{14/15}NH_4^+$ ratio was calculated according to Eq. (1), from the hypobromite oxidation of the NH_4^+ average and the analyses of the produced $^{29}N_2$ and $^{30}N_2$. As the oxidation efficiency of the NH_4^+ is below 100%, the $^{15}NH_4^+$ concentration was calculated from the spectrophotometric NH_4^+ concentration and the $^{15/14}NH_4^+$ ratio, as reported in Eq. (2). The concentration of $^{14}NH_4^+$ was calculated as the difference. The $^{15}NH_4^+$ fluxes can be null or negative due to uptake or oxidation but they cannot be positive. The $^{14}NH_4^+$ fluxes can be positive, null or negative as they integrate production and consumption processes. In the case of negative $^{15}NH_4^+$ fluxes, proportional $^{14}NH_4^+$ uptake was calculated, assuming no significant short-term effect of preferential $^{14}NH_4^+$ over $^{15}NH_4^+$ uptake. From the negative slopes of $^{15}NH_4^+$ fluxes and the $^{15/14}NH_4^+$ ratios, the theoretical $^{14}NH_4^+$ uptake during the incubation was also calculated and combined with net $^{14}NH_4^+$ fluxes to obtain gross $^{14}NH_4^+$ fluxes (Eq. 3). All fluxes (µmol NH_4^+, $^{15}NH_4^+$ or $^{14}NH_4^+$ aggregate^{-1} h^{-1}) were calculated by multiplying concentration versus time slopes by the mesocosm's water volume (in l). From hypobromide oxidation and MIMS:

$$^{15/14}NH_4^+ = \frac{2 \times \left(\sqrt{[^{30}N_2]}\right)}{[^{29}N_2]} \quad (1)$$

from spectrophotometer and MIMS:

$$^{15}NH_4^+ = \frac{([NH_4^+] \times {}^{15/14}NH_4^+)}{1 + {}^{15/14}NH_4^+} \quad (2)$$

and from spectrophotometer and MIMS:

$$[^{14}NH_4^+] = [NH_4^+ - {}^{15}NH_4^+] \quad (3)$$

2.4. Expt 2: Calculation of labelled and unlabelled NO_3^- fluxes and nitrification rates

Surficial sediments from the Goro Lagoon (0–5 cm depth) were used to perform $^{14}NO_3^-$ and $^{15}NO_3^-$ reduction in water samples collected during Expt 2, as described in Carpintero Moraes et al. (2019). *In situ* sediments, rather than pure cultures of denitrifying bacteria or chemical reductions, were chosen due to their elevated denitrification efficiency and absence of anammox (Bartoli et al. 2012, Magri et al. 2020).

As for NH_4^+ flux calculations, a linear regression approach based on the concentration changes of $^{14}NO_3^-$ and $^{15}NO_3^-$ during the experiment, and the dilution of the labelled NO_3^- with the produced unlabelled NO_3^-, was used for the measurement of nitrification rates (μmol N aggregate^{-1} h^{-1}). Fluxes of $^{15}NO_3^-$ can be null or negative due to uptake or reduction. Fluxes of $^{14}NO_3^-$ can be positive, null or negative as they integrate production (nitrification) and consumption processes. The processes of $^{15}NO_3^-$ consumption were assumed to be proportional to those of $^{14}NO_3^-$, assuming no preferential ^{14}N uptake in the short term. All calculations and assumptions are detailed in Carpintero Moraes et al. (2019).

2.5. Measurement of benthic N processes in intact sediment cores underneath and in the proximity of the oyster reef

Intact sediments were collected by hand in plexiglass cores (internal diameter: 4 cm; height: 20 cm) (Fig. 1b). Samples were taken from sediment spots within the oyster reef (hereafter Site Oy; n = 8) and in a control area 400 m from the reef (hereafter Site Ct; n = 8). Collected sediments were levelled to fill half of the core. Both sites had similar muddy-clayish sediment, water chemistry and hydrodynamics (Table S1) (Magri et al. 2020).

Cores were submersed in *in situ* water, transported to the laboratory within 2 h and pre-incubated under dark conditions overnight. Extra cores (n = 3) were collected from both sites for sediment characterization.

Intact core pre-incubation and incubation procedures followed the standardised protocol described in Bartoli et al. (2021). The day following sampling, the water in the tank was replaced with new *in situ* water, and the cores underwent 2 sequential dark incubations. The first incubation was to determine the measurement of net fluxes (O_2 and NH_4^+) and the second was to measure NO_3^- reduction processes (denitrification and dissimilatory nitrate reduction to ammonium [DNRA] rates). Incubations started by sealing the cores with gas-tight lids. The cores were incubated at 10°C for 7 h under continuous stirring, and the incubation time was set to keep O_2 concentration at the end within 20–30% of the initial value (nearly 300 μM). For the first incubation, dissolved O_2 was measured with a microsensor as described earlier, and water samples (20 ml, in quadruplicate) were collected at t_0 from the incubation tank just before sealing the cores. These water samples were filtered (Whatman 0.7 μm GF/F glass fibre filters), transferred to plastic vials and frozen for later NH_4^+ determination. The same procedure was repeated at the end of the incubation, when dissolved O_2 and water samples were measured and collected from each core water phase, respectively. Fluxes of O_2 and NH_4^+ were calculated from the changes in concentration with time, and are expressed as the rate per m^2. Negative fluxes indicate fluxes from the water column to the sediment, while positive fluxes indicate fluxes from sediment to the water column.

After the first incubation, the cores were submerged in renewed *in situ* water for a few hours and then a second incubation started following the revised isotope pairing technique (r-IPT; Risgaard-Petersen et al. 2003). The r-IPT allows for testing the co-occurrence of denitrification and anammox in sediments and for calculations of both rates along with measuring DNRA (Robertson et al. 2019). Moreover, it allows us to differentiate within total denitrification (D_{tot}) the denitrification of NO_3^- diffusing to the anoxic sediment from the water column (D_w) and the denitrification of NO_3^- produced within the sediment due to nitrification (D_n). At the beginning of the experiment, the water in the tank was lowered just below the top of the cores and 2 different amounts of $^{15}NO_3^-$ were added to each core water phase to test whether genuine $^{28}N_2$ production was independent of the $^{15}NO_3^-$ addition (i.e. no anammox in the sediment) (Robertson et al. 2019). At each site, half of the cores were spiked with a $^{15}NO_3^-$ stock solution (10 mM) to a final $^{15}NO_3^-$ concentration of 133 μM, while the other half reached a final $^{15}NO_3^-$ concentration of 163 μM. The cores were then sealed with gas-tight lids and the incubation was started (t_0). At the end of the incubation (t_1), which lasted 7 h, the lids were removed and the sediment and water were gently mixed into a slurry. An aliquot of the slurry was transferred to a 12 ml vial (Exetainer, Labco) and poisoned with 200 μl of 7 M $ZnCl_2$. The abundances of $^{29}N_2$ and $^{30}N_2$ in the pool of dissolved N_2 were analysed via MIMS. As genuine $^{28}N_2$ production was independent of the $^{15}NO_3^-$ concentration, the denitrification rates were calculated according to

the equations of Nielsen (1992). A second sample of slurry (30 ml) was collected from each core and treated with hypobromite as previously described (Magri et al. 2020) to determine DNRA rates. The oxidation of $^{15}NH_4^+$ to $^{29}N_2$ or $^{30}N_2$ followed the protocol described by Warembourg (1993), and the total DNRA rate ($DNRA_{tot}$) was split into the contribution of ammonification of water column nitrate ($DNRA_w$) and ammonification of nitrate produced via nitrification ($DNRA_n$). Calculations and assumptions are reported in Risgaard-Petersen & Rysgaard (1995).

Denitrification efficiency (DE) was calculated both for sediments and oyster holobionts dividing the rates of N_2 production by the sum of N_2 and positive dissolved inorganic nitrogen (DIN) fluxes (NH_4^+ and NO_3^-) (Eyre & Ferguson 2009). A DE of 100% means that the whole pool of mineralized N is converted into molecular N, whereas DE < 100% suggests that part of the mineralised N is recycled to the water column.

2.6. Sediment characterization

Three additional cores per site were used for sediment characterization. Sediments were extruded and sliced into 5 layers: 0–1, 1–2, 2–3, 3–5 and 5–10 cm. Each slice was homogenized and treated as follows: 1 ml of sediment was collected from the 0–1 cm layer via a cut-off syringe, transferred into a 15 ml tube containing 10 ml of 90% acetone and stored for 24 h in the dark at 4°C for chl *a* extraction. The following day, after centrifugation (5 min at 4°C and 864 × *g*), samples were analysed through the spectrophotometer according to Lorenzen (1967). Another subsample of 5 ml was collected from the homogenised sediments at each layer to quantify the physical properties of the sediments. Density (g ml^{-1}) was determined by weighing the fresh sediments; the organic matter content (in %) was measured via loss on ignition (4 h at 550°C in the muffle furnace) (Heiri et al. 2001). The C:N sediment molar ratio together with stable isotopes of C and N ($\delta^{13}C$ and $\delta^{15}N$) were analysed with an elemental analyser (Thermo Electron Corporation FlashEA 1112, Thermo Fisher Scientific) at the Center for Physical Sciences and Technology (Lithuania). Before measurement, samples were acidified with 1 N HCl to remove carbonates.

2.7. Statistical analyses

After verifying test assumptions and plotting residuals for data normality and Levene's test for homogeneity of variance, a 1-way analysis of variance (ANOVA) was used to check differences between O_2 and NH_4^+ fluxes measured in biofilm-coated and cleaned oyster aggregates (Db, Lb and Dc). Additionally, a 2-way ANOVA was used to check differences in organic matter content and sediment density between sites and sediment layers. The Scheirer-Ray-Hare test (Sokal & Rohlf 1995) was used to test for differences between oyster aggregate-mediated denitrification rates (Db vs. Dc) because data did not meet the 2-way ANOVA assumptions (Mangiafico 2023). All other analyses were performed via *t*-test or Wilcoxon test when the normality assumption was not met. Pairwise comparisons after the *t*-test or Wilcoxon test were performed using the 'compare_means()' function within the 'ggpubr' package (Kassambara 2023), whereas pairwise comparisons after ANOVA were performed with the 'emmeans_test()' function within the 'emmeans' package (Lenth et al. 2023). All the graphs were created using 'ggplot2' package (Wickham 2016) and all the analyses were run via the free open-source R software v.4.1.3 (R Core Team 2022).

3. RESULTS

3.1. Expt 1

3.1.1. Oyster holobiont aggregates O_2 and NH_4^+ fluxes

Expt 1 revealed different net O_2 fluxes in the 3 treatments, with average values of −214.4 ± 10.6, −142.8 ± 19.4 and −139.2 ± 7.8 µmol O_2 $aggregate^{-1}$

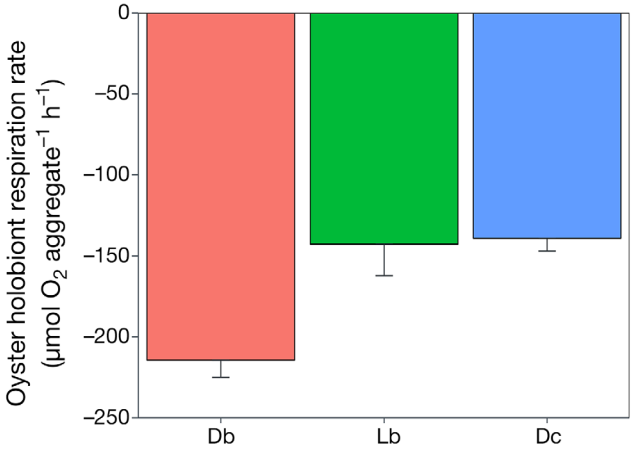

Fig. 2. Mean (±SE) fluxes of O_2 measured in oyster holobiont aggregates in dark biofilm-coated (Db), light biofilm-coated (Lb) and dark cleaned (Dc) treatments. Data derived from Expt 1 (n = 4)

h^{-1} in Db, Lb and Dc, respectively (Fig. 2). Pairwise comparisons detected statistical differences between Db and Dc conditions ($p = 0.01$, $F_{2,9} = 9.82$). The biofilm coating accounted for 35% of the whole oyster holobiont aggregate respiration. Similar chl *a* concentrations in the biofilm of the oysters used in this and the following experiment suggested the presence of active algae (Fig. S4). The oyster aggregate's gross primary production was estimated at 71.6 µmol O_2 aggregate^{-1} h^{-1}. O_2 fluxes measured in Dc, normalised by the mollusc flesh dry biomass, averaged −18.9 ± 1.3 µmol O_2 g_{dw}^{-1} h^{-1}.

Net NH_4^+ fluxes were always positive (from oyster holobiont aggregates to the water column) and averaged 6.6 ± 0.5, 5.25 ± 0.4 and 6.1 ± 0.7 µmol NH_4^+ aggregate^{-1} h^{-1} in Db, Lb and Dc, respectively (Fig. 3b). Despite a tendency toward lower NH_4^+ production in Lb and Dc compared to Db, pairwise comparisons between coupled incubations resulted in no statistical differences ($p = 0.60$, $F_{2,9} = 1.95$). The contribution of the biofilm to the net NH_4^+ production from the oyster holobiont aggregate, calculated from Db and Dc treatments, was 7%. Mollusc biomass-normalised oyster excretion rate, calculated from Dc, averaged 0.82 ± 0.08 µmol NH_4^+ g_{dw}^{-1} h^{-1}.

The ratio of $^{14}NH_4^+$ to $^{15}NH_4^+$ concentrations in the mesocosms of treatments Db and Lb increased throughout the experiment (from 1.49 ± 0.24 to 6.93 ± 1.52, obtained by averaging initial and final ratios of the 2 treatments, Fig. 3a). The slopes of the regression between $^{14}NH_4^+$ to $^{15}NH_4^+$ concentration ratios over time averaged 0.39 ± 0.06, 0.27 ± 0.04 and 0.28 ± 0.02 h^{-1} in Db, Lb and Dc, respectively (Fig. 3a). The pairwise comparison between treatments Db and Dc revealed no significant difference ($p = 0.16$).

The ratio between O_2 and NH_4^+ fluxes measured in Db and Dc averaged 31 and 22, respectively.

3.1.2. Fluxes of $^{15}NH_4^+$ and $^{14}NH_4^+$ in the oyster holobiont aggregates

Throughout the dark and light incubations, the concentration of $^{15}NH_4^+$ decreased in all treatments, with rates of −0.36 ± 0.12, −0.37 ± 0.04 and −0.29 ± 0.04 µmol $^{15}NH_4^+$ aggregate^{-1} h^{-1} in Db, Lb and Dc, respectively (Fig. 3b). Despite a tendency toward lower $^{15}NH_4^+$ consumption in the absence of biofilm, the pairwise comparison between the coupled oyster aggregates, Db and Dc, revealed no statistical differences ($p = 0.63$). Theoretical $^{14}NH_4^+$ uptake rates were calculated from $^{15}NH_4^+$ fluxes. The calculated $^{14}NH_4^+$ uptake was combined with net NH_4^+ fluxes to calculate gross $^{14}NH_4^+$ fluxes that averaged 8.6 ± 1.0, 6.11 ± 0.9 and 7.4 ± 0.7 µmol $^{14}NH_4^+$ aggregate^{-1} h^{-1} in Db, Lb and Dc, respectively (Fig. 3b). No statistical differences were detected between Db and Dc ($p = 0.40$).

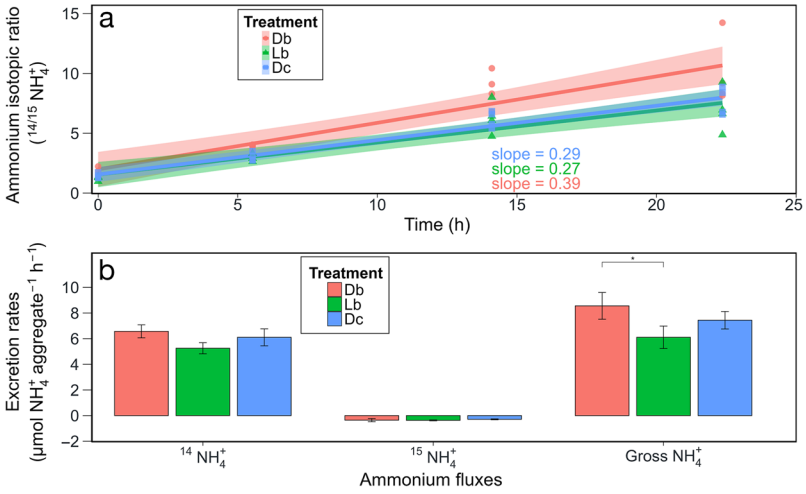

Fig. 3. (a) Trend of $^{14/15}NH_4^+$ ratios throughout incubation of the treatment tested: dark biofilm-coated (Db), light biofilm-coated (Lb) and dark biofilm-cleaned (Dc). Shadows represent 95% confidence interval for each regression. (b) Net NH_4^+ ($^{14}NH_4^+$ + $^{15}NH_4^+$) and $^{15}NH_4^+$ fluxes and calculated gross $^{14}NH_4^+$ production in treatment Db, Lb and Dc. Averages ± SE are reported (n = 4); when present, asterisks indicate a statistically significant difference among treatments (*$p < 0.05$; **$p < 0.01$; ***$p < 0.001$)

3.2. Expt 2

3.2.1. Denitrification rates in oyster holobiont aggregates

Ambient denitrification rates (D_{tot}) averaged 2.75 ± 0.28, 2.29 ± 0.74 and 1.35 ± 0.19 µmol N aggregate^{-1}h^{-1} in Db, Lb and Dc, respectively. Denitrification in Db was significantly higher than in Dc ($p = 0.026$). D_w represented nearly 87 and 77% of D_{tot} in Db and Lb, respectively, whereas in Dc, 100% of denitrification was sustained by D_w (Table 1).

3.2.2. Fluxes of $^{15}NO_3^-$ and $^{14}NO_3^-$ and nitrification rate in oyster holobiont aggregates

The ratio of $^{14}NO_3^-$ to $^{15}NO_3^-$ concentrations in the Db and Lb treatments increased during the experi-

Table 1. Dark and light oxygen (net O_2 flux), ammonium (net NH_4^+ flux), nitrate (net NO_3^- flux) and N_2 (D_w: denitrification rates of water column NO_3^-; D_n: NO_3^- produced via nitrification) fluxes measured in biofilm-coated and cleaned oyster aggregates, and rates of potential ammonification calculated from O_2 fluxes, gross NH_4^+ production calculated from $^{15}NH_4^+$ uptake, nitrification calculated via $^{15}NO_3^-$ dilution and denitrification efficiency (see Sections 2.2–2.4 for calculation details). Db: dark biofilm-coated; Lb: light biofilm-coated; Dc: dark cleaned. Averages ± SE are reported (n = 4)

Process	Treatment			Units
	Db	Lb	Dc	
Net O_2 flux	214.4 ± 10.6	142.8 ± 19.4	139.2 ± 7.8	µmol O_2 aggregate^{-1} h^{-1}
Net NH_4^+ flux	6.6 ± 0.5	5.3 ± 0.4	6.1 ± 0.7	µmol N aggregate^{-1} h^{-1}
Net NO_3^- flux	2.5 ± 1.6	8.4 ± 1.3	4.7 ± 1.0	µmol N aggregate^{-1} h^{-1}
N_2 D_w	2.4 ± 0.2	1.8 ± 0.5	1.4 ± 0.2	µmol N aggregate^{-1} h^{-1}
D_n	0.4 ± 0.1	0.5 ± 0.3	0.0 ± 0.0	
Potential ammonification	30.6 ± 1.5	20.4 ± 2.8	19.9 ± 1.1	µmol N aggregate^{-1} h^{-1}
Gross NH_4^+ production	8.6 ± 1.0	6.1 ± 0.9	7.4 ± 0.7	µmol N aggregate^{-1} h^{-1}
Nitrification	14.8 ± 1.8	21.4 ± 2.0	9.4 ± 2.4	µmol N aggregate^{-1} h^{-1}
Denitrification efficiency	10.7	7.7	10.7	%

ment (from 6.00 ± 0.03 to 7.90 ± 0.18, obtained by averaging the initial and final ratios of the 2 treatments). The slopes of the regression between $^{14}NO_3^-$ and $^{15}NO_3^-$ concentration ratios over time averaged 0.11 ± 0.01, 0.11 ± 0.02 and 0.02 ± 0.02 h^{-1} in Db, Lb and Dc, respectively (Fig. 4a). The pairwise comparison between Db and Dc treatments revealed a significant difference (p = 0.02).

The concentrations of $^{15}NO_3^-$ decreased throughout the experiment in the Db and Lb treatments, with averaged rates of −1.54 ± 0.36 and −0.70 ± 0.25 µmol $^{15}NO_3^-$ aggregate^{-1} h^{-1}, whereas a negligible decrease occurred in Dc $^{15}NO_3^-$ and averaged 0.02 ± 0.38 µmol $^{15}NO_3^-$ aggregate^{-1} h^{-1} (Fig. 4b). The pairwise comparison between Db and Dc treatments revealed no significant difference (p = 0.10), but the tendency revealed higher $^{15}NO_3^-$ depletion (= higher uptake or assimilation) in Db compared to Dc.

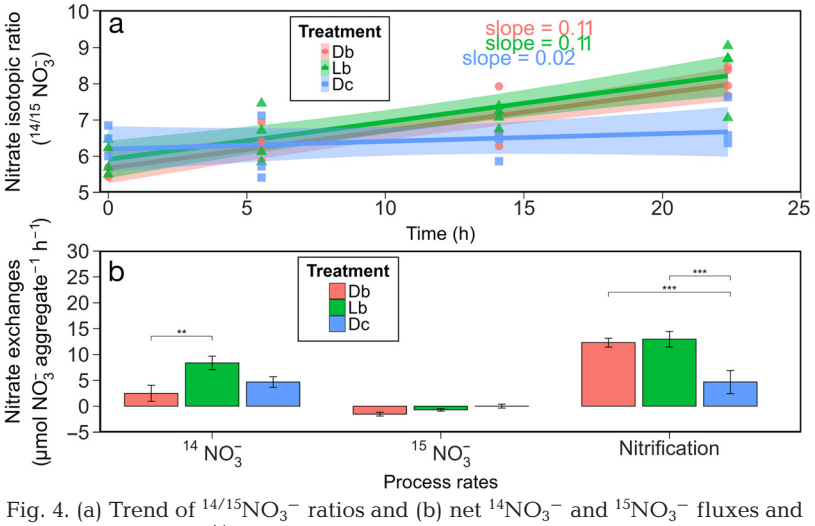

Fig. 4. (a) Trend of $^{14/15}NO_3^-$ ratios and (b) net $^{14}NO_3^-$ and $^{15}NO_3^-$ fluxes and nitrification (gross $^{14}NO_3^-$) in the 3 treatments (see Fig. 3 for further details)

From these rates and the $^{14}NO_3^-$ to $^{15}NO_3^-$ concentration ratios in the mesocosms, it was possible to calculate the $^{14}NO_3^-$ uptake as if no nitrate production occurred, which averaged −1.23 ± 0.28, −0.58 ± 0.21 and 0.01 ± 0.27 µmol $^{14}NO_3^-$ h^{-1}. The pairwise comparison between treatments Dd and Dc revealed a significant difference (p = 0.02), with higher $^{14}NO_3^-$ consumption (= higher uptake, or assimilation, or denitrification) in Db than Dc, suggesting that the biofilm was responsible for a major fraction of $^{14}NO_3^-$ consumption.

The difference between the slopes of net $^{14}NO_3^-$ production (Fig. 4b) and calculated $^{14}NO_3^-$ consumption allowed the calculation of gross $^{14}NO_3^-$ production (i.e. nitrification), which averaged 1.54 ± 0.10, 1.61 ± 0.19 and 0.56 ± 0.27 µM $^{14}NO_3^-$ h^{-1}. The pairwise comparison between treatments Db and Dc revealed a significant difference (p = 0.01), highlighting higher $^{14}NO_3^-$ production (= higher nitrification) in Db than in Dc.

Multiplying the gross $^{14}NO_3^-$ production by the water volume (in l) in the mesocosm, it was possible to calculate the averaged nitrification rates, which averaged 12.30 ± 0.86 (Db), 12.96 ± 1.51 (Lb) and 4.68 ± 2.23 (Dc) µmol $^{14}NO_3^-$ aggregate^{-1}h^{-1} (Fig. 4b). Pairwise comparison between Db and Dc treatment revealed statistical difference (p = 0.02), suggesting that the real NO_3^- production rate can be masked by other assimilative processes occurring within the oyster holobiont.

3.3. Sediment physical features and metabolism

Site Oy had labile, organic sediments, with significantly lower density and higher percentage of organic matter and C and N contents compared to Site Ct (Table 2).

Despite these differences, O_2 consumption and NH_4^+ regeneration were similar at the 2 sites. At Sites Ct and Oy, sediment respiration averaged 732.5 ± 80.0 and 662.2 ± 71.1 µmol O_2 m^{-2} h^{-1}, and NH_4^+ fluxes averaged 25.5 ± 9.0 and 28.8 ± 4.4 µmol NH_4^+ m^{-2} h^{-1}, respectively (Fig. 5a,b). No statistical differences emerged between sediment respiration rates at the 2 sites (p = 0.53) or NH_4^+ fluxes (p = 0.71) (Fig. 5a,b).

3.4. Sediment denitrification and DNRA rates

Calculated ambient denitrification was unaffected by the $^{15}NO_3^-$ addition, suggesting insignificant rates of anammox (Fig. S5). Significantly higher rates of D_w were measured at site Oy, whereas D_n rates were similar at both sites (p < 0.001 and p = 0.26, respectively) (Fig. 5c). Rates of $DNRA_{tot}$ were similar at both sites (p = 0.72). However, while $DNRA_w$ rates showed no differences between sites (p = 0.16), $DNRA_n$ was significantly higher at Site Ct (p = 0.04) than at Site Oy (Fig. 5d).

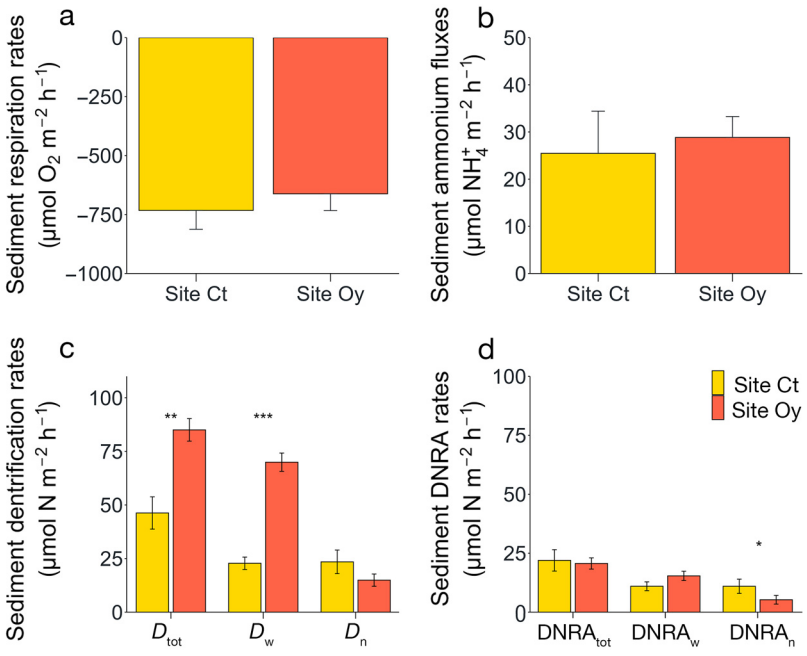

Fig. 5. Mean (±SE) (a) O_2 fluxes at Site Ct (far from the oyster reef) and Site Oy (close to the oyster reef) and (b) NH_4^+ fluxes at the sediment–water interface at both experimental sites. (c,d) Sediment denitrification and dissimilatory nitrate reduction to ammonium (DNRA) rates at the 2 sampling sites (n = 8 $site^{-1}$). Asterisks indicate a statistically significant difference among treatments (*p < 0.05; **p < 0.01; ***p < 0.001)

Table 2. Sediment general features at the sampling sites (Ct: control; Oy: oyster reef). Chlorophyll *a* (chl *a*), carbon (C) and nitrogen (N) content and stable isotopes of C and N ($\delta^{13}C$ and $\delta^{15}N$) were measured only in the surface sediment layer (0–1 cm). Sediment density and organic matter are given, including for additional sediment layers. Values in **bold** indicate a statistically significant difference (*p < 0.05; **p < 0.01; ***p < 0.001). Sediment density ANOVA: $F_{site1,20}$ = 250.23, $F_{layer4,20}$ = 15.22; sediment organic matter $F_{site1,15}$ = 43.46, $F_{layer1,15}$ = 0.34. Averages ± SE (n = 3) are reported

	Chl *a* (mg m^{-2})	C (%)	Sediment features N (%)	$\delta^{13}C$	$\delta^{15}N$
Site Ct	28.3 ± 6.71	**0.79 ± 0.15****	**0.11 ± 0.02****	−24.9 ± 0.13	7.01 ± 0.27
Site Oy	31.7 ± 6.13	**2.08 ± 0.08****	**0.29 ± 0.02****	−25.7 ± 0.23	8.83 ± 1.07
			Sediment density (g ml^{-1})		
Sediment depth (cm)	0–1	1–2	2–3	3–5	5–10
Site Ct	**1.42 ± 0.02*****	**1.55 ± 0.03*****	**1.69 ± 0.09*****	**1.78 ± 0.00*****	**1.81 ± 0.04*****
Site Oy	**1.20 ± 0.04*****	**1.21 ± 0.02*****	**1.27 ± 0.02*****	**1.30 ± 0.01*****	**1.32 ± 0.03*****
			Sediment organic matter (%)		
Sediment depth (cm)	0–1	1–2	2–3	3–5	5–10
Site Ct	**3.39 ± 0.55***	3.06 ± 0.46	**2.35 ± 0.45****	**2.18 ± 0.16****	**1.82 ± 0.09****
Site Oy	**6.26 ± 1.80***	5.38 ± 2.79	**7.01 ± 0.24****	**6.33 ± 0.81****	**6.26 ± 0.04****

The reconstructed benthic N cycle at Sites Ct and Oy is shown in Fig. S6a,b. The potential ammonification within sediments was calculated from O_2 respiration and the sedimentary C:N ratios. Nitrate efflux from sediment was calculated by difference combining potential ammonification, net NH_4^+ efflux from sediment, denitrification and DNRA data. Both sites were net DIN sources to the water column and their DEs were ~35 and ~67% at Sites Ct and Oy, respectively.

4. DISCUSSION

4.1. Dark and light O_2 fluxes in biofilm-coated and cleaned oyster aggregates

Dark incubations of biofilm-coated and cleaned oyster holobiont aggregates revealed that biofilms consumed ~70 µmol O_2 aggregate^{-1} h^{-1}, corresponding to nearly one-third of the whole aggregate respiration (Table 1). If all O_2 consumption by the biofilm is due to nitrifiers, the potential for nitrification by the biofilm is 35 µmol N aggregate^{-1} h^{-1}. As natural oyster reefs may host from ~100 to ~800 ind. m^{-2} (Schulte et al. 2009, Higgins et al. 2013, Windle et al. 2022), the averaged aggregate respiration rates reported in this study, if upscaled to a surface of 1 m^2, should be multiplied by a factor of 25 and 200 (4 oysters per chamber were used on average during incubations). This means that at 10°C, the true dark O_2 uptake of an oyster reef in the Goro Lagoon can vary between 5 and 42 mmol O_2 m^{-2} h^{-1}, of which 35% (1.8–15 mmol O_2 m^{-2} h^{-1}) is consumed by biofilms growing on oyster shells (Fig. 6a). Such a range of respiration rates is nearly 8–64 times higher than the respiration measured in sediments underneath or in the proximity of the reef, confirming that aggregates are significantly larger O_2 sinks than sediments (Melià et al. 2003, Nizzoli et al. 2007, Volaric et al. 2020). During summer months, when water temperatures in the Goro Lagoon exceed 25°C and O_2 saturation is below 250 µM, such respiration rates would lead to hypoxia or anoxia events and oyster mortality. Anoxia is reported for this lagoon due to the high biomass of cultivated clams, stimulating macroalgal blooms and collapse events, whereas the contribution of oysters to the O_2 budget has never been considered (Viaroli et al. 2001, Bartoli et al. 2003, Naldi et al. 2020). Oyster respiration rates reported in this study fall within biomass-normalised or areal ranges reported in the literature. For example, summer oyster reef respiration rates ranged between 12.5 and 20.3 mmol O_2 m^{-2} h^{-1} at densities between 186 and 350 oysters m^{-2} (Volaric et al. 2018). Respiration rates overlapping those from this study are reported in a seasonal study by Volaric et al. (2020), ranging between 2.3 and 11.5 mmol O_2 m^{-2} h^{-1}, and by Reidenbach et al. (2013), ranging between 4.2 and 25 mmol O_2 m^{-2} h^{-1}. Higher respiration rates were found using experimental chambers, as in the present work, ranging from 28.2 to 38.8 mmol O_2 m^{-2} h^{-1} (Kellogg et al. 2013, 2014, Humphries et al. 2016). Measurements carried out in the light and dark highlight the active role of benthic algae growing on sediments in the proximity of oyster reefs or on oyster shells (Volaric et al. 2020). However, these measurements also confirm that reefs are strongly heterotrophic and that O_2 production constitutes a minor part of total respiration (Dame et al. 1992, Volaric et al. 2020). The heterotrophic nature of reefs suggests a net production and release to the water column of inorganic nutrients, resulting from direct excretion and organic matter mineralization (Dame 1999, Bartoli et al. 2001, Smyth et al. 2016, Smaal et al. 2019).

In our experiments, light incubations of biofilm-coated aggregates did not reverse O_2 fluxes, which remained negative, with net consumption rates comparable to those measured in cleaned aggregates (Table 1). The calculated gross photosynthetic production (75 µmol O_2 m^{-2} h^{-1}) represents nearly one-third of the whole oyster holobiont respiration. Benthic microalgal production in shallow environments affects the N cycle (Varela & Penas 1985, Rysgaard et al. 1995, Eyre & Ferguson 2002). Algal uptake of the excreted N from the oyster holobionts may lower net NH_4^+ flux during light. It can also inhibit nitrification due to competition between microalgae and microbes for inorganic N or the production of allelopathic substances (Nils 2003, Risgaard-Petersen et al. 2004). Algal photosynthesis produces other indirect but important effects on N-related microbial processes. For example, it can expand the O_2 penetration in the biofilm, reducing anoxic niches and impairing N loss via denitrification in the light (Nielsen et al. 1990). As biofilms growing on shells are extremely thin (on the scale of µm) and given that active microphytobenthos can increase O_2 penetration in sediments by 1–2 mm, the activity of microalgae can turn the biofilm oxic, stimulating nitrification and suppressing denitrification. Table 3 provides a compilation, taken from the literature, of cleaned-oyster respiration rates. Oyster respiration measured in the present study aligns with previously published data. The ratio of dark O_2 to NH_4^+ fluxes calculated with data from the present work varied between 22 and 31 for Dc and Db aggregates, respectively—values that are 3–4 times higher

Table 3. Oyster respiration rates measured in this study and extracted from previously published works normalized per gram of oyster flesh dry weight. When present, averages ± SE are reported

Species	Water temperature (°C)	Respiration rate (μmol O_2 g_{dw}^{-1} h^{-1})	Reference
Magallana gigas	10	18.9 ± 1.3	This study
M. gigas	8–17	19.1 ± 6.4	Bougrier et al. (1995)
M. gigas	20	13.8 ± 8.5	Goulletquer et al. (1999)
Pinctada mazatlantica	18–23	4.3 ± 0.5	Saucedo et al. (2004)
M. gigas	10–20	7.2 ± 4.2	Dunphy et al. (2006)
M. gigas	10–12	5.4 ± 1.0	Lejart et al. (2012)
M. virginica	24	1.4 ± 0.3	Ray et al. (2019)
M. gigas	15	23.4	Le Moullac et al. (2007)
M. gigas	16	40.6	Boucher & Boucher-Rodoni (1988)
Ostrea edulis	18 ± 1	26.6–42.2	Albentosa et al. (2023)
M. corteziensis	23	155.7 ± 72.6	Guzmán-Agüero et al. (2013)

than the theoretical Redfield reference. However, the measured O_2 fluxes may include a fraction of O_2 consumed to oxidise NH_4^+ via nitrification, which needs to be removed from the calculations. Additionally, net NH_4^+ fluxes do not include the fraction of NH_4^+ produced by the aggregate, which is nitrified. This fraction should be included and accounted for in the calculations. Implementing such a correction would lead to a decrease in the numerator (net O_2 fluxes − O_2 used by nitrification) and an increase in the denominator (net NH_4^+ fluxes + NH_4^+ nitrified), resulting in a lower ratio. These issues are discussed in detail in Section 4.2, as nitrification was measured with the $^{15}NO_3^-$ dilution technique and the O_2 consumed by nitrifiers was calculated accordingly. Calculated O_2 to NH_4^+ ratios from laboratory or *in situ* oyster incubations are extremely heterogeneous and vary between 9, relatively close to the Redfield ratio, and 121 (Boucher & Boucher-Rodoni 1988, Saucedo et al. 2004, Guzmán-Agüero et al. 2013). The latter value may suggest an unrealistic organic matter source to oysters with a very high C:N ratio or that the NH_4^+ excreted is immediately oxidised or assimilated.

4.2. Dark and light N fluxes in biofilm-coated and cleaned oyster aggregates

All treatments net released NH_4^+ to the water column at comparable rates (5.3–6.6 μmol N aggregate^{-1} h^{-1}) (Table 1). There was a tendency toward lower fluxes in Dc than in Db, but this difference was not significant and did not reflect the significant drop of O_2 fluxes in the absence of biofilms. Indeed, NH_4^+ in the Dc treatment was only 7% lower than in Db. This result can be interpreted in terms of much higher nitrification in Db compared to Dc, converting NH_4^+ into NO_3^-, carried out in the aerobic volume of the biofilms and resulting in lower NH_4^+ net release to the water column. Indeed, results from the $^{15}NO_3^-$ dilution experiment suggest significantly higher nitrification in biofilm-coated than in cleaned oyster holobiont (Table 1). Also, in Lb, net NH_4^+ fluxes were reduced compared to the Db condition, likely due to a combination of photosynthetic uptake and higher nitrification rates stimulated by higher O_2 availability (Smith et al. 2014).

In Table 1, the rates of nitrification calculated with the $^{15}NO_3^-$ dilution technique can be discussed within the framework of other N-related processes occurring in the oyster aggregates. As nitrification converts NH_4^+ into NO_3^-, this process is supported by NH_4^+ production. In Db, it can be speculated that nearly 15 out of 31 μmol of NH_4^+ potentially produced (50%) by the oyster holobiont are nitrified, whereas nearly 7 μmol (22%) were net released to the water column (Table 1). In Lb, nitrification has the potential to oxidise 100% of the NH_4^+ potentially produced by the oyster holobiont and nearly 5 μmol (25%) were net released (Table 1). Finally, less than half of the NH_4^+ potentially excreted by cleaned oyster holobionts was oxidised and 30% was net released (Table 1). Taken together, these results suggest that higher nitrification rates occur in the light on biofilm-coated oyster holobionts and that such rates are reduced in the dark due to relatively low O_2 availability within the biofilm and in cleaned aggregates due to the removal of the biofilm. They also suggest that a major fraction of nitrification occurs within the oyster holobiont. In Db, nitrification is not set to zero, suggesting that nitrifiers are likely growing along the molluscs' syphons, in their gills and other oxic tissues such as the mantle cavity. Different studies report the presence of potential or directly measured nitrifying activity inside mol-

luscs (Caffrey et al. 2016 and references therein). Microbiome analysis was not carried out in this work; however, bioinformatics data supported the presence of genes and microbes actively involved in N cycling in the presence of oysters (Arfken et al. 2017). Moreover, *in situ* trophic conditions seem to drive the abundance and functional plasticity of those genes (Stevick et al. 2021).

Denitrification in oyster holobionts was mainly sustained by water column NO_3^- diffusing into anoxic microniches, with rates decreasing from Db to Lb to Dc (Table 1). Comparatively, D_n had a much lower importance and was quantitatively much lower than nitrification rates (or even null, in Dc) (Table 1). A possible explanation for this result is that nitrification occurred in fully oxic niches that were not adjacent to anoxic counterparts. As a result, the produced NO_3^- was either assimilated or released into the water. Denitrification associated with the oyster holobionts represented a small fraction (23–42%) of net NH_4^+ fluxes and a minor fraction (15–19%) of the NO_3^- produced via nitrification. Denitrification efficiency calculated for the 3 treatments was very similar and close to 10% (Table 1). This observation implies that in February, oyster holobionts in the Goro Lagoon, whether exposed to light or in darkness and with or without biofilms, contributed significantly to recycling a substantial portion of the N they process back into the water column.

This result, of course, cannot be generalised because it was produced from a single study carried out in February. It is important to consider that despite assumptions and approximations, the reported N budget is realistic and is supported by the 2 experiments involving the use of both $^{15}NH_4^+$ and $^{15}NO_3^-$. Moreover, the inventory of the measured inorganic N transformations fits with the calculated potential NH_4^+ production derived from O_2 fluxes (Table 1). Indeed, the measured NH_4^+ fluxes plus the nitrification rates (21.4 ± 1.8, 27.5 ± 2.2 and 16.8 ± 2.5 µmol N aggregate^{-1} h^{-1}) represent 70 ± 10, 135 ± 29 and 85 ± 17% of the calculated potential ammonification rates (30.6 ± 1.5, 20.4 ± 2.8 and 19.9 ± 1.1 µmol NH_4^+ aggregate^{-1} h^{-1}) in Db, Lb and Dc, respectively. As 2 mol of O_2 are needed to oxidise one mol of NH_4^+ to NO_3^-, and because nitrification rates can be added to net NH_4^+ fluxes to calculate true NH_4^+ production, the O_2 respiration to NH_4^+ excretion ratios are 7.9 ± 1.2, 3.6 ± 1.0 and 7.2 ± 1.6 for Db, Lb and Dc, respectively. All these ratios are very close to the theoretical Redfield ratio for phytoplankton (Redfield 1934). Furthermore, the ratio between O_2 and NH_4^+ fluxes measured in Db and Dc averaged 31 and 22, respectively. Such a difference suggests dark NH_4^+ uptake or oxidation (e.g. nitrification) by the biofilm in Db. As oysters primarily feed on phytoplankton with a theoretical C:N ratio of ~7, the calculated ratio for Dc suggests either other food sources for oysters in the Goro Lagoon or the occurrence of NH_4^+ retention or oxidation processes within the oysters.

If results at the aggregate level are upscaled to the square meter level to compare oyster-mediated N cycling with sedimentary N dynamics, such an upscaling procedure would not change the already reported DE of oyster holobionts but would allow comparison of denitrification rates measured in sediments with denitrification rates in 1 m^2 of oyster aggregates.

The approach we used here is very conservative; indeed, much higher oyster densities are also reported, over 2000 ind. m^{-2}, from reefs that likely develop vertically in well-flushed marine systems but are unlikely in the microtidal Goro Lagoon (Windle et al. 2022). This means that rates of O_2 or N fluxes at sites with variable densities within this range align with the ranges reported in Fig. 6. Upscaled rates of O_2 respiration, NH_4^+ excretion, nitrification and denitrification in oyster reefs fall within rates reported in the literature. Upscaling individual rates measured in summer by Caffrey et al. (2016) revealed O_2 consumption ranging from 1.79 to 14.14 mmol O_2 m^{-2} h^{-1}, NH_4^+ production from 0.34 to 2.71 mmol NH_4^+ m^{-2} h^{-1} and N removal via denitrification at rates from 0.03 to 0.25 mmol N m^{-2} h^{-1}. Our upscaled rates are lower than those measured in November on a restored reef by Kellogg et al. (2013), who reported rates of O_2 consumption ranging from 9.8 to 77.62 mmol O_2 m^{-2} h^{-1}, NH_4^+ production from 0.5 to 3.96 mmol NH_4^+ m^{-2} h^{-1} and rates of N removal via denitrification from 0.2 to 1.58 mmol N m^{-2} h^{-1}. Lower NH_4^+ recycling rates (0.57–4.54 mmol NH_4^+ m^{-2} h^{-1}) but higher denitrification rates (0.48–3.79 mmol N m^{-2} h^{-1}) are reported in the meta-analysis carried out by Ray & Fulweiler (2021). By contrast, Arfken et al. (2017) reported a denitrification rate of 0.36 mmol N m^{-2} h^{-1}, similar to that reported in this study.

4.3. Biomass-normalised oyster excretion rates

The average NH_4^+ excretion rate by biofilm-free oysters measured in our experiments at 10°C was 0.8 ± 0.1 µmol NH_4^+ g_{dw}^{-1} h^{-1}, a value slightly lower than other rates reported in the literature. As stated for respiration rates, differences in oyster species or temperature range could partially explain the variations

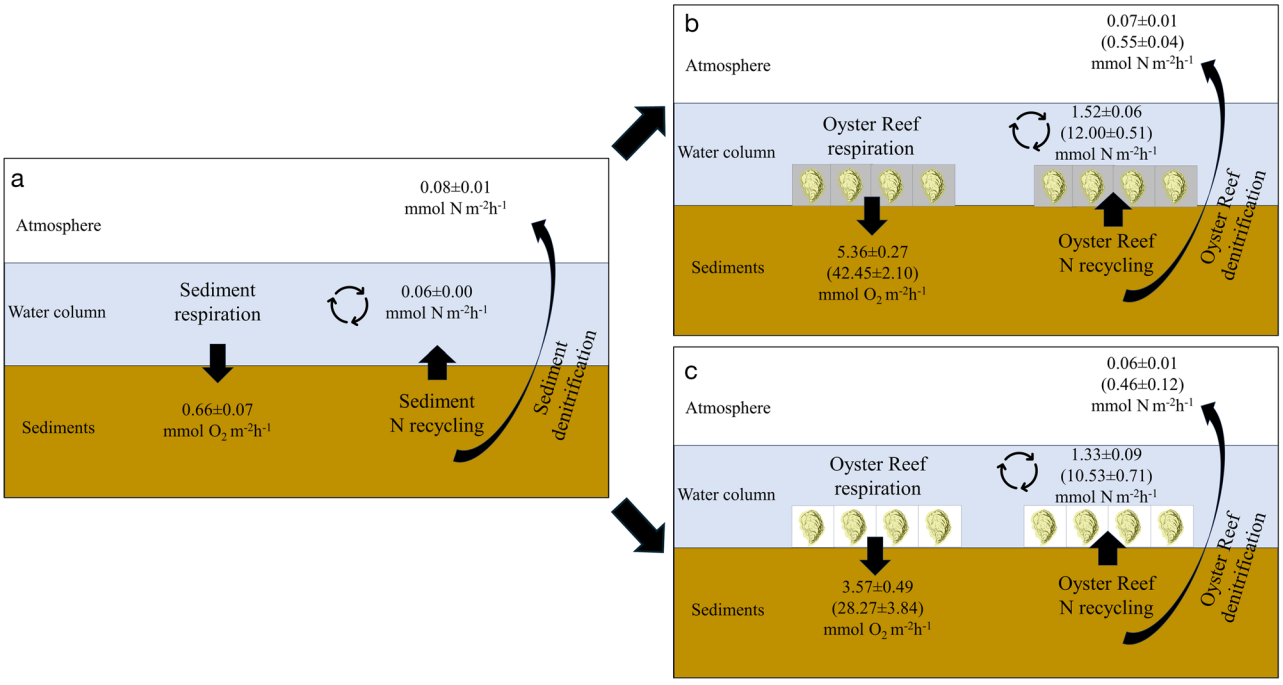

Fig. 6. Fluxes of inorganic N in Goro Lagoon sediments hosting oyster reefs. Fluxes display 3 benthic processes: O_2 respiration, N recycling and N removal from the system via denitrification. (a) Processes mediated by the sediment underneath the oyster reef; (b,c) integrating the oyster reef contribution in dark and light incubation, respectively. Rates (mean ± SE) measured in oyster aggregates were upscaled using low (100 ind. m^{-2}) and high (800 ind. m^{-2}, in parentheses) oyster densities, as reported in the literature

between our data and those in the literature. For example, NH_4^+ excretion rates of 1.3 ± 0.2, 2.4 ± 0.7 and 2.2 ± 0.3 µmol NH_4^+ g_{dw}^{-1} h^{-1} were measured at 7.7, 12.4 and 13.5°C, respectively for *Magallana* (*Crassostrea*) *gigas* (Mao et al. 2006). In another study on the same species at 11°C, Regnault et al. (1988) reported a rate of 1.3 ± 0.3 µmol NH_4^+ g_{dw}^{-1} h^{-1}. Boucher & Boucher-Rodoni (1988) found rates of 0.3 and 4.6 µmol NH_4^+ g_{dw}^{-1} h^{-1} in winter and summer, respectively. Lower excretion rates, such as 0.2 and 0.5 µmol NH_4^+ g_{dw}^{-1} h^{-1} at 13 and 16°C, respectively, were observed for *M. gigas* in France (Buzin et al. 2015), and for *M. virginica* at 24°C, 0.2 ± 0.1 µmol NH_4^+ g_{dw}^{-1} h^{-1} (Ray et al. 2019). Moreover, different oyster species showed higher NH_4^+ excretion rates, such as rates up to 2.4 µmol NH_4^+ g_{dw}^{-1} h^{-1} for *M. corteziensis* at temperatures ranging from 23 to 32°C (Guzmán-Agüero et al. 2013), or 2.5 µmol NH_4^+ g_{dw}^{-1} h^{-1} for *Saccostrea glomerata* at 20°C (Erler et al. 2017).

4.4. Reef versus bare sediment O_2 and N fluxes

The comparison between oyster aggregates and sediment metabolism, after upscaling rates to a surface of 1 m^2, is reported in Fig. 6. These processes are seldom measured simultaneously (Caffrey et al. 2016). Considering the 2 extremes of oyster biomass, the presence of oysters over sediments results in a stimulation of O_2 demand by a factor of 8–64, a stimulation of NH_4^+ mobilisation of 25–200 and a stimulation of denitrification by ~1–7. Similar studies carried out in different environments, seasons and oyster densities have reported comparatively high stimulation of community respiration by ~2–11 (Filippini et al. 2023), NH_4^+ mobilisation by ~1–29 (Kellogg et al. 2013, Filippini et al. 2023) and denitrification by ~0.5–24 (Arfken et al. 2017, Ray & Fulweiler 2021 and references therein). By contrast, Hoellein & Zarnoch (2014) found no oyster influence on N fluxes.

Overall, oyster reefs in the Goro Lagoon in February had a major effect on NH_4^+ recycling, then on O_2 respiration and denitrification rates. Although oysters stimulate denitrification, the extent of stimulation is lower than that of recycling. In the microtidal and eutrophic Goro Lagoon, high oyster biomass can foster the risk of local anoxia and represent a biological reactor for the phytoplankton delivered to the lagoon by the Po di Volano River. Oysters play a crucial role in retaining phytoplankton, preventing its export to the open sea and converting it into biomass, biodeposits and excreted nutrients as NH_4^+.

The latter serves as an N source for microalgae growing on oyster shells, in the water column and over the sediment surface as well as for macroalgae. Previous studies focusing on clam cultivation in the Goro Lagoon postulated that in semi-enclosed, low-flushed systems such as this lagoon, cultivated molluscs represent a potential threat due to their large O_2 consumption, substantial production and limited export of biodeposits, and local nutrient recycling, favouring (macro)algal growth. It is essential to note that these results are based on observations from a single season and should be repeated during warmer months. Caution is advised regarding the use of oysters as providers of biogeochemical ecosystem services or nature-based solutions.

Acknowledgements. The present work is part of S.P.'s PhD thesis. S.P. was supported by a doctoral fellowship (funded by the project Dipartimenti Universitari di eccellenza 2018 _2022, SCVSA_2018-2022_DIP_ECCELLENZA, cod CUP - D91G18000140001). We thank Leonardo Morini, Monia Magri, Luca Bellini and Emilie Le Floch'h for their assistance during field and lab activities. This research benefited from the equipment and framework of the COMP-R Initiative, funded by the 'Departments of Excellence' program of the Italian Ministry for University and Research (MUR, 2023–2027).

LITERATURE CITED

Albentosa M, Akinyemi MI, Vera M, Ibarrola I, Filgueira R, Galimany E, Martínez P (2023) Recovery of eutrophized marine ecosystems using the European flat oyster, *Ostrea edulis*. Aquat Conserv: Mar Freshw Ecosyst

APHA (American Public Health Association) (1975) Standard methods for the examination of water and wastewater, 14th edn. American Public Health Association, Washington, DC

Arfken A, Song B, Bowman JS, Piehler M (2017) Denitrification potential of the eastern oyster microbiome using a 16S rRNA gene based metabolic inference approach. PLOS ONE 12:e0185071

Ayvazian S, Mulvaney K, Zarnoch C, Palta M and others (2021) Beyond bioextraction: the role of oyster-mediated denitrification in nutrient management. Environ Sci Technol 55:14457–14465

Bartoli M, Nizzoli D, Viaroli P, Turolla E, Castaldelli G, Fano EA, Rossi R (2001) Impact of *Tapes philippinarum* farming on nutrient dynamics and benthic respiration in the Sacca di Goro. Hydrobiologia 455:203–212

Bartoli M, Naldi M, Nizzoli D, Roubaix V, Viaroli P (2003) Influence of clam farming on macroalgal growth: a microcosm experiment. Chem Ecol 19:147–160

Bartoli M, Castaldelli G, Nizzoli D, Viaroli P (2012) Benthic primary production and bacterial denitrification in a Mediterranean eutrophic coastal lagoon. J Exp Mar Biol Ecol 438:41–51

Bartoli M, Benelli S, Lauro M, Magri M, Vybernaite-Lubiene I, Petkuviene J (2021) Variable oxygen levels lead to variable stoichiometry of benthic nutrient fluxes in a hypertrophic estuary. Estuar Coast 44:689–703

Bernard FR, Noakes DJ (1990) Pumping rates, water pressures, and oxygen use in eight species of marine bivalve molluscs from British Columbia. Can J Fish Aquat Sci 47: 1302–1306

Boucher G, Boucher-Rodoni R (1988) *In situ* measurement of respiratory metabolism and nitrogen fluxes at the interface of oyster beds. Mar Ecol Prog Ser 44:229–238

Bougrier S, Geairon P, Deslous-Paoli JM, Bacher C, Jonquières G (1995) Allometric relationships and effects of temperature on clearance and oxygen consumption rates of *Crassostrea gigas* (Thunberg). Aquaculture 134: 143–154

Bower CE, Holm-Hansen T (1980) A salicylate–hypochlorite method for determining ammonia in seawater. Can J Fish Aquat Sci 37:794–798

Buzin F, Dupuy B, Lefebvre S, Barillé L, Haure J (2015) Storage of Pacific oysters *Crassostrea gigas* in recirculating tank: ammonia excretion and potential nitrification rates. Aquacult Eng 64:8–14

Caffrey JM, Hollibaugh JT, Mortazavi B (2016) Living oysters and their shells as sites of nitrification and denitrification. Mar Pollut Bull 112:86–90

Carpintero Moraes P, Arroyave Gòmez DM, Vincenzi F, Castaldelli G, Fano EA, Bartoli M, Benelli S (2019) Analysis of $^{15}N–NO_3^-$ via anoxic slurries coupled to MIMS analysis: an application to estimate nitrification by burrowing macrofauna. Water 11:2310

Chambers LG, Gaspar SA, Pilato CJ, Steinmuller HE, McCarthy KJ, Sacks PE, Walters LJ (2018) How well do restored intertidal oyster reefs support key biogeochemical properties in a coastal lagoon? Estuar Coast 41: 784–799

Dalsgaard T, Nielsen LP, Brotas V, Viaroli P and others (2000) Protocol handbook for NICE — nitrogen cycling in estuaries: a project under the EU research programme. Marine Science and Technology (MAST III). National Environmental Research Institute, Silkeborg

Dame RF (1999) Oyster reefs as components in estuarine nutrient cycling: Incidental or regulating? In: Luckenbach MW, Mann R, Wesson JA (eds) Oyster reef habitat restoration: a synopsis and synthesis of approaches. Virginia Institute of Marine Science Press, Gloucester Point, VA, p 267–280

Dame RF, Spurrier JD, Zingmark RG (1992) *In situ* metabolism of an oyster reef. J Exp Mar Biol Ecol 164:147–159

Dunphy BJ, Wells RM, Jeffs AG (2006) Oxygen consumption and enzyme activity of the subtidal flat oyster (*Ostrea chilensis*) and intertidal Pacific oyster (*Crassostrea gigas*): responses to temperature and starvation. NZ J Mar Freshw Res 40:149–158

Erler DV, Welsh DT, Bennet WW, Meziane T, Hubas C, Nizzoli D, Ferguson AJ (2017) The impact of suspended oyster farming on nitrogen cycling and nitrous oxide production in a sub-tropical Australian estuary. Estuar Coast Shelf Sci 192:117–127

Eyre BD, Ferguson AJP (2002) Comparison of carbon production and decomposition, benthic nutrient fluxes and denitrification in seagrass, phytoplankton, benthic microalgae- and macroalgae-dominated warm-temperate Australian lagoons. Mar Ecol Prog Ser 229:43–59

Eyre BD, Ferguson AJ (2009) Denitrification efficiency for defining critical loads of carbon in shallow coastal ecosystems. In: Andersen JH, Conley DJ (eds) Eutrophica-

tion in coastal ecosystems: towards better understanding and management strategies. Developments in Hydrobiology, Vol 207. Springer, Dordrecht, p 137–146
Filippini G, Bugnot AB, Ferguson A, Gribben PE, Palmer J, Erickson K, Dafforn KA (2023) The influence of oyster reefs and surrounding sediments on nitrogen removal — an *in-situ* study along the East coast of Australia. Environ Res 237:116947
Goulletquer P, Wolowicz M, Latala A, Geairon P, Huvet A, Boudry P (1999) Comparative analysis of oxygen consumption rates between cupped oyster spat of *Crassostrea gigas* of French, Japanese, Spanish and Taiwanese origins. Aquat Living Resour 12:271–277
Gutiérrez JL, Jones CG, Strayer DL, Iribarne OO (2003) Mollusks as ecosystem engineers: the role of shell production in aquatic habitats. Oikos 101:79–90
Guzmán-Agüero JE, Nieves-Soto M, Hurtado MÁ, Pina-Valdez P, Garza-Aguirre MDC (2013) Feeding physiology and scope for growth of the oyster *Crassostrea corteziensis* (Hertlein, 1951) acclimated to different conditions of temperature and salinity. Aquacult Int 21:283–297
Haven DS, Morales-Alamo R (1966) Aspects of biodeposition by oysters and other invertebrate filter feeders. Limnol Oceanogr 11:487–498
Heiri O, Lotter AF, Lemcke G (2001) Loss on ignition as a method for estimating organic and carbonate content in sediments: reproducibility and comparability of results. J Paleolimnol 25:101–110
Higgins CB, Tobias C, Piehler MF, Smyth AR, Dame RF, Stephenson K, Brown BL (2013) Effect of aquacultured oyster biodeposition on sediment N_2 production in Chesapeake Bay. Mar Ecol Prog Ser 473:7–27
Hoellein TJ, Zarnoch CB (2014) Effect of eastern oysters (*Crassostrea virginica*) on sediment carbon and nitrogen dynamics in an urban estuary. Ecol Appl 24:271–286
Humphries AT, Ayvazian SG, Carey JC, Hancock BT and others (2016) Directly measured denitrification reveals oyster aquaculture and restored oyster reefs remove nitrogen at comparable high rates. Front Mar Sci 3:74
Ivanov V, Stabnikova O, Sihanonth P, Menasveta P (2006) Aggregation of ammonia-oxidizing bacteria in microbial biofilm on oyster shell surface. World J Microbiol Biotechnol 22:807–812
Jørgensen BB, Wenzhöfer F, Egger M, Glud RN (2022) Sediment oxygen consumption: role in the global marine carbon cycle. Earth Sci Rev 228:103987
Kana TM, Darkangelo C, Hunt MD, Oldham JB, Bennett GE, Cornwell JC (1994) Membrane inlet mass spectrometer for rapid high-precision determination of N_2, O_2, and Ar in environmental water samples. Anal Chem 66: 4166–4170
Karlson K, Hulth S, Ringdahl K, Rosenberg R (2005) Experimental recolonisation of Baltic Sea reduced sediments: survival of benthic macrofauna and effects on nutrient cycling. Mar Ecol Prog Ser 294:35–49
Kassambara A (2023) ggpubr: 'ggplot2' based publication ready plots. R package version 0.6.0. https://CRAN.R-project.org/web/packages/ggpubr/index.html
Kellogg ML, Cornwell JC, Owens MS, Paynter KT (2013) Denitrification and nutrient assimilation on a restored oyster reef. Mar Ecol Prog Ser 480:1–19
Kellogg ML, Cornwell JC, Owens MS, Luckenbach MW, Ross PG, Leggett TA (2014) Scaling ecosystem services to reef development: effects of oyster density on nitrogen removal and reef community structure. Virginia Institute of Marine Science, College of William & Mary, Gloucester Point, VA
Kemp WM, Sampou P, Caffrey J, Mayer M, Henriksen K, Boynton WR (1990) Ammonium recycling versus denitrification in Chesapeake Bay sediments. Limnol Oceanogr 35:1545–1563
Le Moullac G, Quéau I, Le Souchu P, Pouvreau S, Moal J, René Le Coz J, Samain JF (2007) Metabolic adjustments in the oyster *Crassostrea gigas* according to oxygen level and temperature. Mar Biol Res 3:357–366
Lenth RV, Banfai B, Bolker B, Buekner P and others (2023) emmeans: estimated marginal means, aka least-squares means. R package version 1.8.8. https://CRAN.R-project.org/package=emmeans
Lejart M, Clavier J, Chauvaud L, Hily C (2012) Respiration and calcification of *Crassostrea gigas*: contribution of an intertidal invasive species to coastal ecosystem CO_2 fluxes. Estuar Coast 35:622–632
Lorenzen CJ (1967) Determination of chlorophyll and pheopigments: spectrophotometric equations. Limnol Oceanogr 12:343–346
Magri M, Benelli S, Bonaglia S, Zilius M, Castaldelli G, Bartoli M (2020) The effects of hydrological extremes on denitrification, dissimilatory nitrate reduction to ammonium (DNRA) and mineralization in a coastal lagoon. Sci Total Environ 740:140169
Mangiafico S (2023) rcompanion: functions to support extension education program evaluation. R package version 2.4.34. https://CRAN.R-project.org/package=rcompanion
Mao Y, Zhou Y, Yang H, Wang R (2006) Seasonal variation in metabolism of cultured Pacific oyster, *Crassostrea gigas*, in Sanggou Bay, China. Aquaculture 253:322–333
McCarthy JJ (1980) Nitrogen. In: Morris I (ed) The physiological ecology of phytoplankton. University of California Press, Berkeley, CA, p 191–233
McMahon RF, Williams CJ (1984) A unique respiratory adaptation to emersion in the introduced Asian freshwater clam *Corbicula fluminea* (Müller) (Lamellibranchia: Corbiculacea). Physiol Zool 57:274–279
Melià P, Nizzoli D, Bartoli M, Naldi M, Gatto M, Viaroli P (2003) Assessing the potential impact of clam rearing in dystrophic lagoons: an integrated oxygen balance. Chem Ecol 19:129–146
Michaud E, Desrosiers G, Mermillod-Blondin F, Sundby B, Stora G (2006) The functional group approach to bioturbation. II. The effects of the *Macoma balthica* community on fluxes of nutrients and dissolved organic carbon across the sediment–water interface. J Exp Mar Biol Ecol 337:178–189
Michaud E, Desrosiers G, Aller RC, Mermillod-Blondin F, Sundby B, Stora G (2009) Spatial interactions in the *Macoma balthica* community control biogeochemical fluxes at the sediment–water interface and microbial abundances. J Mar Res 67:43–70
Mo C, Neilson B (1994) Standardization of oyster soft tissue dry weight measurements. Water Res 28:243–246
Murphy AE, Nizzoli D, Bartoli M, Smyth AR, Castaldelli G, Anderson IC (2018) Variation in benthic metabolism and nitrogen cycling across clam aquaculture sites. Mar Pollut Bull 127:524–535
Murphy AE, Kolkmeyer R, Song B, Anderson IC, Bowen J (2019) Bioreactivity and microbiome of biodeposits from filter-feeding bivalves. Microb Ecol 77:343–357

Naldi M, Nizzoli D, Bartoli M, Viaroli P, Viaroli P (2020) Effect of filter-feeding mollusks on growth of green macroalgae and nutrient cycling in a heavily exploited coastal lagoon. Estuar Coast Shelf Sci 239:106679

Nielsen LP (1992) Denitrification in sediment determined from nitrogen isotope pairing. FEMS Microbiol Lett 86: 357–362

Nielsen LP, Christensen PB, Revsbech NP, Sørensen J (1990) Denitrification and oxygen respiration in biofilms studied with a microsensor for nitrous oxide and oxygen. Microb Ecol 19:63–72

Nils RP (2003) Coupled nitrification–denitrification in autotrophic and heterotrophic estuarine sediments: on the influence of benthic microalgae. Limnol Oceanogr 48: 93–105

Nizzoli D, Bartoli M, Viaroli P (2006a) Nitrogen and phosphorous budgets during a farming cycle of the Manila clam *Ruditapes philippinarum*: an *in situ* experiment. Aquaculture 261:98–108

Nizzoli D, Welsh DT, Fano EA, Viaroli P (2006b) Impact of clam and mussel (*Tapes philippinarum* and *Mytilus galloprovincialis*) farming on benthic metabolism and nitrogen cycling, with emphasis on nitrate reduction pathways. Mar Ecol Prog Ser 315:151–165

Nizzoli D, Bartoli M, Viaroli P (2007) Oxygen and ammonium dynamics during a farming cycle of the bivalve *Tapes philippinarum.* Hydrobiologia 587:25–36

Norkko A, Villnäs A, Norkko J, Valanko S, Pilditch C (2013) Size matters: implications of the loss of large individuals for ecosystem function. Sci Rep 3:2646

R Core Team (2022) R: a language and environment for statistical computing. R Foundation for Statistical Computing, Vienna

Ray NE, Fulweiler RW (2021) Meta-analysis of oyster impacts on coastal biogeochemistry. Nat Sustain 4:261–269

Ray NE, Henning MC, Fulweiler RW (2019) Nitrogen and phosphorus cycling in the digestive system and shell biofilm of the eastern oyster *Crassostrea virginica.* Mar Ecol Prog Ser 621:95–105

Redfield AC (1934) On the proportions of organic derivatives in sea water and their relation to the composition of plankton. In: Nicholson AJ (ed) James Johnstone Memorial Volume. University Press of Liverpool, Liverpool, p 176–192

Regnault M, Boucher-Rodoni R, Boucher G, Lasserre P (1988) Effects of macrofauna excretion and turbulence on inorganic nitrogenous exchanges at the water–sediment interface. Experimental approach in microcosms. Cah Biol Mar 29:427–444

Reidenbach MA, Berg P, Hume A, Hansen JCR, Whitman ER (2013) Hydrodynamics of intertidal oyster reefs: the influence of boundary layer flow processes on sediment and oxygen exchange. Limnol Oceanogr Fluids Environ 3:225–239

Reise K (1983) Biotic enrichment of intertidal sediments by experimental aggregates of the deposit-feeding bivalve *Macoma balthica.* Mar Ecol Prog Ser 12:229–236

Richard M, Archambault P, Thouzeau G, Desrosiers G (2006) Influence of suspended mussel lines on the biogeochemical fluxes in adjacent water in the Îles-de-la-Madeleine (Quebec, Canada). Can J Fish Aquat Sci 63:1198–1213

Risgaard-Petersen N, Rysgaard S (1995) Nitrate reduction in sediments and waterlogged soil measured by ^{15}N techniques. In: Alef K, Nannipieri P (eds) Methods in applied soil microbiology. Academic Press, London, p 1–13

Risgaard-Petersen N, Nielsen LP, Rysgaard S, Dalsgaard T, Meyer RL (2003) Application of the isotope pairing technique in sediments where anammox and denitrification coexist. Limnol Oceanogr Methods 1:63–73

Risgaard-Petersen N, Nicolaisen MH, Revsbech NP, Lomstein BA (2004) Competition between ammonia-oxidizing bacteria and benthic microalgae. Appl Environ Microbiol 70: 5528–5537

Robertson EK, Bartoli M, Brüchert V, Dalsgaard T, Hall PO, Hellemann D, Conley DJ (2019) Application of the isotope pairing technique in sediments: use, challenges, and new directions. Limnol Oceanogr Methods 17:112–136

Rose JM, Gosnell JS, Bricker S, Brush MJ and others (2021) Opportunities and challenges for including oyster-mediated denitrification in nitrogen management plans. Estuar Coast 44:2041–2055

Rysgaard S, Christensen PB, Nielsen LP (1995) Seasonal variation in nitrification and denitrification in estuarine sediment colonized by benthic microalgae and bioturbating infauna. Mar Ecol Prog Ser 126:111–121

Saucedo PE, Ocampo L, Monteforte M, Bervera H (2004) Effect of temperature on oxygen consumption and ammonia excretion in the Calafia mother-of-pearl oyster, *Pinctada mazatlanica* (Hanley, 1856). Aquaculture 229: 377–387

Schulte DM, Burke RP, Lipcius RN (2009) Unprecedented restoration of a native oyster metapopulation. Science 325:1124–1128

Searles AR, Gipson EE, Walters LJ, Cook GS (2022) Oyster reef restoration facilitates the recovery of macroinvertebrate abundance, diversity, and composition in estuarine communities. Sci Rep 12:8163

Smaal AC, Ferreira JG, Grant J, Petersen JK, Strand Ø (eds) (2019) Goods and services of marine bivalves. Springer, Cham

Smith JM, Chavez FP, Francis CA (2014) Ammonium uptake by phytoplankton regulates nitrification in the sunlit ocean. PLOS ONE 9:e108173

Smyth AR, Geraldi NR, Thompson SP, Piehler MF (2016) Biological activity exceeds biogenic structure in influencing sediment nitrogen cycling in experimental oyster reefs. Mar Ecol Prog Ser 560:173–183

Sokal RR, Rohlf FJ (1995) Biometry, 3rd edn. WH Freeman, New York, NY

Stevick RJ, Post AF, Gómez-Chiarri M (2021) Functional plasticity in oyster gut microbiomes along a eutrophication gradient in an urbanized estuary. Anim Microbiome 3:5

Stief P (2013) Stimulation of microbial nitrogen cycling in aquatic ecosystems by benthic macrofauna: mechanisms and environmental implications. Biogeosciences 10: 7829–7846

Sundbäck K, Miles A, Göransson E (2000) Nitrogen fluxes, denitrification and the role of microphytobenthos in microtidal shallow-water sediments: an annual study. Mar Ecol Prog Ser 200:59–76

Takeda S (1998) Influence of iron availability on nutrient consumption ratio of diatoms in oceanic waters. Nature 393:774–777

Trottet A, Leboulanger C, Vidussi F, Pete R, Bouvy M, Fouilland E (2016) Heterotrophic bacteria show weak competition for nitrogen in Mediterranean coastal waters (Thau Lagoon) in autumn. Microb Ecol 71:304–314

Vachon D, Sadro S, Bogard MJ, Lapierre JF and others (2020) Paired O_2–CO_2 measurements provide emergent in-

sights into aquatic ecosystem function. Limnol Oceanogr Lett 5:287–294

Varela M, Penas E (1985) Primary production of benthic microalgae in an intertidal sand flat of the Ria de Arosa, NW Spain. Mar Ecol Prog Ser 25:111–119

Viaroli P, Azzoni R, Bartoli M, Giordani G, Tajé L (2001) Evolution of the trophic conditions and dystrophic outbreaks in the Sacca di Goro lagoon (Northern Adriatic Sea). In: Faranda FM, Guglielmo L, Spezie G (eds) Mediterranean ecosystems: structures and processes. Springer, Milan, p 467–475

Viaroli P, Giordani G, Bartoli M, Naldi M and others (2006) The Sacca di Goro lagoon and an arm of the Po River. In: Wangersky PJ (ed) Estuaries. The handbook of environmental chemistry, Vol 5H. Springer, Berlin, p 197–232

Volaric MP, Berg P, Reidenbach MA (2018) Oxygen metabolism of intertidal oyster reefs measured by aquatic eddy covariance. Mar Ecol Prog Ser 599:75–91

Volaric MP, Berg P, Reidenbach MA (2020) Drivers of oyster reef ecosystem metabolism measured across multiple timescales. Estuar Coast 43:2034–2045

Warembourg FR (1993) Nitrogen fixation in soil and plant systems. In: Knowles R, Blackburn TH (eds) Nitrogen isotope techniques. Academic Press, New York, NY, p 127–156

Welsh DT, Nizzoli D, Fano EA, Viaroli P (2015) Direct contribution of clams (*Ruditapes philippinarum*) to benthic fluxes, nitrification, denitrification and nitrous oxide emission in a farmed sediment. Estuar Coast Shelf Sci 154:84–93

Wickham H (2016) ggplot2: elegant graphics for data analysis. Springer-Verlag, New York, NY

Windle AE, Puckett B, Huebert KB, Knorek Z, Johnston DW, Ridge JT (2022) Estimation of intertidal oyster reef density using spectral and structural characteristics derived from unoccupied aircraft systems and structure from motion photogrammetry. Remote Sens 14:2163

Yin G, Hou L, Liu M, Liu Z, Gardner WS (2014) A novel membrane inlet mass spectrometer method to measure $^{15}NH_4^+$ for isotope-enrichment experiments in aquatic ecosystems. Environ Sci Technol 48:9555–9562

Yu L, Gan J (2021) Mitigation of eutrophication and hypoxia through oyster aquaculture: an ecosystem model evaluation off the Pearl River Estuary. Environ Sci Technol 55: 5506–5514

Zilius M, Daunys D, Petkuviene J, Bartoli M (2012) Sediment-water oxygen, ammonium and soluble reactive phosphorus fluxes in a turbid freshwater estuary (Curonian lagoon, Lithuania): evidences of benthic microalgal activity. J Limnol 71:309–319

Editorial responsibility: Just Cebrian, Daphne, Alabama, USA
Reviewed by: 2 anonymous referees

Submitted: February 15, 2024
Accepted: December 3, 2024
Proofs received from author(s): January 22, 2025